Journal of Materials Chemistry A

Accepted Manuscript

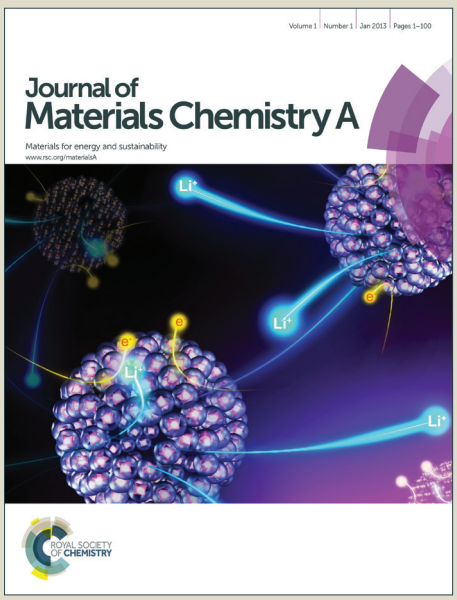

ROYAL SOCIETY OF CHEMISTRY

www.rsc.org/materialsA

High-performance supercapacitor electrode based on nanofibers polyaniline/3D graphene framework as efficient charge transporter

Sachin B. Kulkarni[†], Umakant M. Patil[†], Iman Shackery[†], Ji Soo Sohn, Suchan Lee, Byeongho Park, SeongChan Jun*

Nano ElectroMechanical Device Laboratory, School of Mechanical Engineering, Yonsei University, Seoul 120-749, Republic of Korea.

Abstract

Current paper describes chemically grown polyaniline (PANI) nanofibers on porous three dimensional graphene (PANI/3D Graphene) as a supercapacitor electrode material with enhanced electrochemical performance. The chemical, structural properties of electrode are characterized by X-ray Diffraction (XRD), X-ray Photoelectron spectroscopy (XPS) and Raman spectroscopy with confirmation of semi crystalline nature. The homogeneous growth of PANI on the 3D graphene network is visualized by field emission scanning electron microscopy (FESEM) with nanofibers morphology. The maximum specific capacitance of PANI/3D graphene electrode is found to be ~1024 Fg^{-1} in 1M H_2SO_4 within the potential window -150 to 800 mV vs Ag/AgCl at 10 mV s^{-1} scan rate (~1002 Fg^{-1} at 1 $mAcm^{-2}$ discharge current density). The high surface area offered by conducting, porous 3D graphene framework stimulates effective utilization of deposited PANI and communally improve electrochemical charge transport and storage. Hence, signifying that 3D graphene framework is proficient contender for high-performance capacitor electrodes in energy storage applications.

Keywords: Nanofibers, PANI/3D graphene, Efficient charge transporter, Supercapacitor.

---

† **These authors contributed equally.**

***Corresponding Author*:** SeongChan Jun Email: scj@yonsei.ac.kr

Tel: +82-2-2123-5817; **Fax:** +82-2-312-2159

---

1. Introduction

Supercapacitors are a promising class of electrochemical energy devices for storing and releasing energies speedily and reversibly hence attracted a great interest as an intermediate system between dielectric capacitors and batteries. Mainly carbonaceous material, metal oxides/hydroxides and conducting polymers are studied for the supercapacitor electrode.[1] Conducting polymers have recognized as potential electrode materials attracted great attention due to their high accessible surface area, low resistance, high stability and other fascinating properties. Polymers usually grow in three-dimensional structures which introduce high porosity and roughness, which generates a large surface area favourable for enhancing electrochemical reaction.[2] Polyaniline (PANI) is one of the most extensively used conducting polymers for engineering pseudocapacitors. PANI has multiple redox states, high doping–de doping rate during charge–discharge and good environmental stability. Moreover, it can be economically and easily fabricated into various nanostructures.[3]

Recent researchers attracted much attention on nanostructured carbonaceous materials like carbon nanotubes (CNTs).[4] But graphene based materials show many advantages such as low production cost, high surface area, and excellent conductivity

than CNTs.[5] Graphene has received remarkable attention with exceptional thermal, mechanical, electrical and electrochemical properties. Moreover, graphene is one of the fascinated emerging carbon nanomaterial and can be considered as an ideal electrode material due to its very high theoretical surface area (2630 m^2 g^{-1}). Also it has remarkable electrical conductance which exhibits superior electrochemical properties, such as large potential window, low charge-transfer resistance, excellent electrochemical activity, fast electron transfer rate, etc. The charge carriers in graphene can move for micro meters without scattering under room temperature conditions. Besides, the fast electron transfer between graphene and analyte molecules supports the direct rather than mediated electrochemical reaction.

Graphene has promising suitability in electrochemical field as every atom is a surface atom in a graphene sheet, thus molecular interaction and electron transport through graphene can be exceedingly sensitive to adsorbed molecules.[6] In this concern, it is assumed that, graphene shows great capability in charge transport and storage mechanism than the conventional electrodes. These reinforcing characteristics open up a wide range of potential applications and great interest in developing multifunctional graphene based electrode materials.[7] However, strong π-π interaction causes agglomeration of graphene sheets which thoroughly restricts its practical applications.[8]

Though, only few reports are related to the application of 3D graphene based materials in supercapacitors. Chen et al practised a continuous three-dimensionally interconnected graphene framework deposited by chemical vapour deposition (CVD).[9] Tai et al also showed higher supercapacitive performance (334 Fg^{-1}) of 3D graphene/polyaniline composite hydrogel via a self-assembled method followed by in situ polymerization of aniline.[10] Hence, such an innovative 3D graphene framework is

supposed to remove some intrinsic problems regarding 2D graphene sheets and thus widely extends the strength of graphene in various applications. Herein, we proposed that continuous 3D graphene offers large surface area with a highly conducting network due to absence of inter sheet junction resistance for charge transfer and is mainly advantageous for energy storage.[11-13] The large specific surface area (SSA) and the conductive robust structure of 3D graphene usually assist the charge transfer, redox reaction and impose the mechanical strengths of resulting anchored redox active materials with improvement in performance. Such electrode system can allow a facile flow of electronic charges and also improves the interfacial properties between electrode and electrolyte. The presence of porous 3D graphene framework upsurges the specific area of the nanofibers polyaniline, also increases and thereby improves the electrochemical properties.

Here, we showed that the 3D graphene-based polymer (i.e. PANI) electrode abundantly allows simultaneous enhancement in pseudocapacitance and charge transport and storage processes. Therefore, 3D graphene is one of the most capable resources for fabricating the electrodes of pseudo-capacitive materials.

2. Experimental

Two stages are preferred for fabrication of self-supported PANI on 3D graphene framework (GF). In first stage, the preparation of the GF covers chemical vapour deposition (CVD) growth of graphene on Ni foam followed by Ni etching by etchant. The details are described in reference.[9] The second stage comprises deposition of nanofibrous PANI characteristically prepared by rapid mixing of aniline or anilinium salts, in aqueous acidic medium with ammonium per sulfate (APS) via chemical

oxidative polymerization. Hydrogen atoms abstracted from the aniline molecules during their coupling to oligomeric and release polymeric structures.

Chemical oxidation of aniline is carried out at high acidity in 1M sulfuric acid. Aqueous solution of 0.4M aniline monomers is prepared in 1M H_2SO_4 solution. Then 0.1M ammonium per sulfate (APS) in deionized water (D.I.) as an oxidizing agent is used for oxidative polymerization. Both solutions are rapidly mixed together in same proportion at room temperature. Subsequently, a piece of 3D GF is immersed (2 X 4 cm^2) vertically in the prepared solution bath. After the reaction, the green layer is observed onto 3D GF sample approved the formation of thin PANI growth as shown in **figure 1 (a)**.

The thin PANI/3D graphene as electrode material is further characterized for physic-chemical properties studies. The X-ray diffraction (XRD) was carried out on a Rigaku Ultima diffractometer using Cu-Kα radiation. The X-ray photoelectron spectroscopy (XPS) measurements were carried out on a thermo scientific ESCALAB 250 (Thermo Fisher Scientific, UK). Raman spectrum was recorded at ambient temperature on a WITeck CRM200 confocal microscopy Raman system with 488 nm wavelength laser. The morphology of the deposit was reviewed by field-emission scanning electron microscopy (FESEM, JSM-7001F, JEOL). A supercapacitor performance studied by forming the conventional half-test cell comprises three-electrode system includes with PANI/3Dgraphene as working electrode (W.E.), Ag/AgCl as reference electrode (R.E.) and platinum (Pt) as counter electrode (C.E.) in aqueous 1M H_2SO_4 electrolyte. The cyclic voltammetry (CV), galvanostatic charge/discharge tests and EIS measurements were performed using ZIVE SP2 LAB analytical equipment (South Korea) for electrochemical studies.

3. Results and discussion

3.1 Chemical synthesis of PANI/3D graphene electrode

In chemical deposition of PANI, positively charged monomers (e.g. aniline nitrenium cation) were favoured to adsorb on the negatively charged 3D graphene surface by electrostatic and/or π-π stacking interactions between the PANI backbone and the 3D graphene surface.[14] So, the favourably polymerization is occurred on to the more and more nucleation sites facilitated by large SSA of 3D graphene network for continuous deposition of the PANI with good surface coverage (as shown in photograph, **figure 1(a)**). Since PANI is synthesized on 3D graphene via in situ polymerization and give rise to good surface coverage of PANI and the strong π-π interaction. Also, for comparison a commercial stainless steel (SS) substrate was used as the conventional electrode for supercapacitive evaluation with porous 3D graphene.

Normally, when operating in acidic solutions, the induction period shortens with the acid concentration and successively the acidity of the medium upsurges.[15] In this chemical oxidative polymerization via rapid mixing, induction period becomes shorter when any solid material having a high surface area, is introduced in the reaction mixture, such as silica gel, graphite, carbon nanotubes or 3D graphene. Then adsorption of oligomer nucleates on such substrates for which material surface area and hydrophilicity is important.[16, 17]

The origin of the nanofibers PANI structures involves following three successive steps: (a) Nucleates generation, (b) Their organization afforded by adsorption at various surfaces and interfaces via transportation of ions/atoms/molecules/ to nucleation sites (herein 3D graphene) and (c) Growth of PANI chains from organized

nucleates. In the construction of one-dimensional nanostructures, π-π interaction is the main driving force responsible to stabilize columnar stacks produced by nucleates. They are responsible for the subsequent formation of other PANI nanostructures, such as thin films, coatings, etc. From the single stack of nucleates PANI chains grow perpendicular and there form the body of a nanofiber. The development of nanofibers is favoured over the start of new nanofibers in the homogeneous phase. New nucleates are probably produced directly on the front of the growing nanofiber, thus extending its one-dimensional columnar structure. The polymerization of aniline is heterogeneous in nature. Due to limited solubility of nucleates in water hence renovate organized or adsorbed before they change to initiation centres. The PANI chains growth originates from insoluble nucleate clusters or nucleates seeded at dipped surfaces. The stacked nucleates yield nanofibers and the adsorption of nucleates on to the immersed surfaces in the reaction bath later results in thin coating. The reactions and growth schematic is illustrated in **figure 1 (b**) .[14] The monomeric aniline transforms to anilinium cation ($C_6H_5NH_3^+$) in acidic media and further fastly react with oxidant to form intermediate protofibrils aniline nitrenium cation ($C_6H_5NH^+$). Nucleation occurs on sites offered by 3D graphene via chemical oxidative polymerization mechanism and can acts as a 'seed' to accelerate the kinetics of fiber formation within short induction time and avoid further overgrowth.

3.2Structural studies (XRD, XPS and Raman)

Figure 2 illustrates the X-ray diffraction (XRD) pattern of PANI/3D GF sample. The two characteristics diffraction peaks (2θ) at ~26.5° and ~44.5° are reflections from crystalline peak of hexagonal graphite carbon marked as '$' (JCPDS: 75-1621). The peak at 26.5° is characteristic reflection from (002) the parallel graphene layers, whereas the

44.5° (100) diffraction peak corresponds to the 2D in-plane symmetry along the graphene sheets.[18] However, characteristic peaks of the polymer at (2θ) 13.6°, 20.2° and ~25° are the reflections from (011), (020) and (200) planes marked as 'o' reveal semi crystalline nature of deposited PANI on 3D graphene framework, which are in good agreement with previously reported results. Semi crystalline nature of PANI can be attributed to peaks at (2θ) ~20° and ~25° denote the periodicities parallel (100) and perpendicular (110) to the PANI chain respectively.[19 20] When 3D graphene framework was immersed in the solution bath of PANI matrix, the sharp and strong diffraction peak of graphene at (26.5°) was observed as overlap with the peak of PANI which results in the broad and intense peak. The data shows that no extra crystalline order has been introduced in sample. The noticeable characteristic peaks in PANI/3D GF can be recognized to the formation of crystal appearing on the outer layers of 3D graphene framework. This result reveals homogeneous coating of PANI onto the 3D graphene. Organic-inorganic, ions, molecules and other atomic clusters can be loaded onto the basal plane of graphene via complexation reactions or charge-transfer adsorption. Therefore, graphene decorated with these methods can be highly conductive. Hence, these can be effectively applicable in engineering innovative electrode materials for sensors.[21] However, XRD pattern of PANI on SS is (**ESI figure S1**) showing very small peaks except stainless steel peaks marked by '*' indicating lesser semi-crystalline PANI formation as compare to PANI/3D GF.

The XPS study was carried out to evaluate the surface electronic state and the composition of the sample. **Figure 3** showed XPS spectra of chemically deposited PANI on 3D graphene. The atomic composition of sample contained carbon (C), nitrogen (N), oxygen (O) and sulfur (S), as expected. Atomic composition of the PANI/3D graphene

comprises C(1s)=70.94, O(1s)=14.82, N(1s)=8.97, and S(2p)=3.23 At.%, respectively. The deposition of PANI was confirmed by the appearance of a peaks at 399.48 eV assigned to the nitrogen band (N1s) and presence of sulphur (168.48 eV) S(2p) indicated well doped PANI, as shown in **figure 3 (a)** which assists the successful polymerization of aniline in acidic H_2SO_4 on to 3D graphene surface. The highest atomic percent of carbon is significantly originated from 3D graphene backbone. The deconvoluted profile fit of XPS for C(1s) showed presence of C-C/C-H (284.4 eV), C-N/C=N (285.24 eV), C-O (286.22 eV) and C=O (288.85 eV) bonding as shown in **figure 3 (b)**. The XPS N(1s) core–level spectra can be deconvoluted into three peaks as shown in **figure 3 (c)**. The major benzenoid-amine component (-NH-) peak is observed at 399.52 eV along with a small quinoid-imine (=NH-) peak at 398.92 eV. The shoulder peak at high binding energy about 400.84 eV is ascribed to positively charged nitrogen (-NH^+-) which confirms that, some nitrogen (N) has been transmuted into protonated nitrogen species (N^+).[22, 23]

Raman spectroscopy is a powerful tool used to characterize the microstructure of nanosized materials. **Figure 4** shows the Raman spectrum of PANI/3D GF sample exhibit three prominent peaks at ~1340, ~1574 and ~2700 cm^{-1}. The characteristic peaks at ~1574 and ~2700 cm^{-1} corresponding to the G, 2D bands of graphene, respectively.[24, 25] The distinctive peak at ~1340 cm^{-1} can be ascribed to characteristic of PANI. This is in good agreement with earlier reports.[26]

3.3Morphological studies

The nanofibers and nanotubes produced during the synthesis of conducting polymers have received pronounced attention. The rapid mixing of oxidant and

monomer solutions avoids overgrowth of PANI. Total oxidant is quickly consumed while polymerization and unusable after nanofiber formation which restricts additional polymerization responsible for overgrowth. The FESEM micrographs in **figure 5** visualize about the microstructural growth of PANI on 3D GF electrode by chemical deposition method. **Figure 5 (a)** shows FESEM image of a wide porous pristine graphene framework skeleton at a low magnification. The twigs of graphene foam specifying a clear fragment surface with more enlarged view in **figure 5 (b & C),** respectively. **Figure 5 (d)** noticeably revealed the chemically grown PANI all over the 3D GF surface. This overgrowth can be ascribed to a nucleation and coalescence process. The magnified portion of sample is shown in **figure 5 (e)**. The spongy and well covered PANI growth can be easily observed on the backbone of 3D graphene in **figure 5 (f)**. While, **figure 5 (g & h)** displayed the over grown nanofibers PANI. Nanofibers are one-dimensional objects with a diameter typically 20–100 nm. They have a high aspect ratio and are often branched and produce more complex hierarchical structures.[27, 28] The magnified FESEM image **figure 5 (i)** demonstrate the average diameter of PANI nanofiber building blocks can be identified less than 100 nm. Such nanofibers like morphology leads to a high specific surface area which, provides the structural foundation for the high specific capacitance and reduces the diffusion resistance of the electrolyte into electrode matrix hence, it is more advantageous in supercapacitor application.[29] Though, FESEM image of PANI on SS (**ESI figure S2**) clearly indicate agglomerated nanofibers, which is in support with XRD for reduced semi crystalline PANI growth.

3.4Electrochemical studies

The electrochemical characteristics of the nanofibers PANI/3D GF electrode was evaluated by the cyclic voltammetry (CV), galvanostatic charge-discharge and electrochemical impedance spectroscopy (EIS) tests to calculate electrochemical capacitance of electrode. All experiments were carried out in a three compartment cell with a working electrode (PANI/3D GF), a platinum wire (Pt) counter electrode and a Ag/AgCl as reference electrode in 1M H_2SO_4.

3.4.1Cyclic voltammetry

Figure 6 (a) shows comparative cyclic voltammograms of chemically deposited PANI on stainless steel (SS) and 3D graphene framework (GF) as electrode in aqueous 1M H_2SO_4 electrolyte at 50 mV s^{-1} scan rate within optimized voltage window of -0.150 to 0.800 V Vs Ag/AgCl. The electrochemical response currents of the CV curves of both PANI/SS and PANI/3D GF electrodes clearly showed that, the positive sweeps are nearly mirror-images symmetric to their corresponding counterparts on the negative sweeps with reference to the zero-current line. The curves displayed prominent characteristic peaks occur within voltage ranges are usually evidence of pseudocapacitive behaviour which specify capacitive behaviour and is distinct from rectangular shape of ideal capacitors with no resistance.[30] The current under curve is significantly higher for PANI/3D GF than that of PANI/SS electrode. Hence, recommends the supremacy of PANI/3D GF as potential electrode for supercapacitor. Further, **figure 6 (b)** shows the voltammetric responses of PANI/3D GF electrode at different scan rates. As the scan rate increases, the current under curve rises successively with slight changes in CV shape, and rapid current response on voltage reversal occurs at each end potential at all

the scan rates, which shows good electrochemical capacitive nature for the nanofibers PANI/3D GF. Also it is seen that, the CVs represent broad anodic and cathodic peaks at ~0.54 and ~0.12 V are the oxidation reduction peaks indicating redox nature. Also, peak potentials shifted towards more positive and negative values for oxidation and reduction processes, respectively. Thus, the capacitance of PANI/3D GF is psuedocapacitive, mainly aroused from Faradaic reactions of PANI on the graphene surface while the capacitance of graphene framework is conquered by the electric double-layer capacitance. The **figure 6 (c)** indicates redox peak current densities versus the square root of potential scan rates. I_p is peak current density. I_{pa} and I_{pc} denote the anodic (oxidation) and cathodic (reduction) peak current densities. The peak current densities are proportional to the square root of the scan rates, intending that direct proportion between voltammetry current and scan rate and the electrochemical reaction of PANI/3D GF in 1M H_2SO_4 solution is a diffusion-controlled process and hence signify an ideally capacitive behaviour.

The scan rate dependent interfacial and specific capacitance of PANI/3D GF electrode in 1M H_2SO_4 is shown in **figure 6 (d)**. The interfacial and specific capacitance values are decreased from 0.317 to 0.217 Fcm^{-2} and 1024 to 700 Fg^{-1}, respectively, with the scan rate is increased from 10 to 100 mV s^{-1}. The decrease in capacitance value in accordance with the scan rate can be attributed to the presence of inner active sites, which cannot precede the redox transitions completely; probably due to the diffusion effect of proton within the electrode at higher scan rate of CV.[30, 31]

3.4.2Galvanostatic charge discharge

Figure 7 (a) shows comparative galvanostatic charge-discharge (GCD) plots of PANI/SS and PANI/3D GF within potential range of -0.150 to 0.8 V at constant charging current of 1 $mAcm^{-2}$. The characteristic curve of potential variation with cycling time of PANI/3D GF electrode are more prominent and ascribed as redox characteristics in the charge-discharge curve which are directly related to the redox peaks in the CV curves. Also, the charge profile is symmetric and curved, suggesting a pseudocapacitive characteristic of electrode and good supercapacitive behaviour. The comparative examination of GCD curves point out about resistive drop (iR) of PANI/SS (~0.447 V) is substantial than that of PANI/3D GF (~0.066 V) electrode. PANI/3D GF electrode shows approximately more than seven (~7) times less iR drop showing more proficiency as an electrode material for supercapacitor. Obviously, the impeccably interconnected 3D graphene framework offers much better conduction pathways for charge transportation. The maximum specific capacitance values 1002 and 435 Fg^{-1} are observed for PANI/3D GF and PANI/SS electrodes, respectively. The Cs value of 3D graphene based PANI is much higher than that of commercial SS based.

Figure 7 (b) demonstrates the typical GCD plots of the nanofibers PANI/3D GF at various charging current densities as indicated. The non-linear charge–discharge profile of PANI/3D GF electrode, differs from the usual linearity of voltage with time, typically revealed by EDLCs, confirms redox reaction and pseudocapacitive nature. The discharge profile of PANI/3D GF has two distinct stages. The voltage range of 0.8 to 0.4 V is relatively fast discharge rate originated by double-layer capacitance and 0.4 to -0.15 V is a slow discharge rate is reinforced by both double-layer and pseudo capacitance.[32]

The charging current density dependent interfacial and specific capacitance of PANI/3D GF electrode in 1M H_2SO_4 is shown in **figure 7 (c)**. It is clearly seen that, interfacial and specific capacitance values of PANI/3D GF decrease with increase in current density from 0.311 to 0.215 Fcm^{-2} and 1002 to 695 Fg^{-1}, respectively. The large specific surface area, obviously, is highly favourable to achieve high specific capacity as it can provide more electrochemically active sites. At higher charging rates, a surface confined redox process is occurred, which indicates the limitation arising from charge transfer kinetics resulted from less contribution of active electrode materials.

The high-rate dischargeability (HRD) of the electrode is defined as the ratio of discharge capacitance at 4 $mAcm^{-2}$ to that of 1 $mAcm^{-2}$ and calculated by using following formula,

$$HRD(\%) = (C_{S4} / C_{S1}) \times 100 \quad (1)$$

where, C_{S4} and C_{S1} are the discharge specific capacitance (Cs) of the electrode at 4 $mAcm^{-2}$ and 1 $mAcm^{-2}$, respectively. For PANI/3D GF electrode HRD is found to be ~70% demonstrating its better rate capability.[33] The porous 3D graphene structure offers abundant electrolyte ions to swiftly interact with the surfaces of more electroactive PANI nanofibers.

Ragone plot is shown in **figure 7 (d)** relative to the corresponding energy and power densities was calculated from the galvanostatic charge-discharge, with current densities of 1 to 4 $mAcm^{-2}$.[30] The electrical parameters such as, specific power (SP), specific energy (SE) for PANI/3D GF at 1 $mAcm^{-2}$ is found to be ~3 kW kg^{-1}, ~120 Wh kg^{-1}, respectively. It is observed that, time periods of charge and discharges are almost the same, which means high reversibility and high coulombic efficiency. The coulombic

efficiency of nanofibers PANI/3D GF electrode at different current densities is calculated and plotted as shown in **inset of figure 7 (d)**. The coulombic efficiencies at different current densities are all more than 92% and even up to more than 96% when the current densities are not less than 2 $mAcm^{-2}$, revealing the good electrochemical reversibility.

3.4.3Electrochemical stability study

The cycling life of nanofibers PANI/3D GF electrode in 1M H_2SO_4 electrolyte is one of the imperative facets for application point of view. As shown in **figure 8 (a)**, after continuous 5000 charge-discharge cycles at current density of 4 $mAcm^{-2}$. Capacity retention is found to be ~86.5% after 5,000 cycles which, demonstrates the significant electrochemical stability of PANI/3D GF electrode. Capacity retention ratio for PANI/3D GF electrode up to 5,000 cycles was tested by GCD cycles as shown in **inset of figure 8 (a)**. The reduction in specific capacitance can be ascribed to fairly deterioration of PANI after many swelling and shrinking cycles.[32-34] Such a low Cs degradation of suggests the good electrochemical stability of the nanofibers PANI/3D GF. The GF contribute more to the improved cycling stability and excellent rate capability because, it can offer higher surface area of active PANI nanofibers, and maintain the electrical contact to PANI nanofibers during the cycling also, hence resulting in improved cyclic stability.

3.4.4Electrochemical Impedance spectroscopy (EIS)

To better understand the enormous benefit of the 3D graphene framework in supercapacitor, the EIS measurement was employed with open circuit potential (OCP) over the frequency range of 10 MHz and 0.01 Hz and were compared for both PANI/SS and PANI/3D GF electrodes. To confirm the good conductivity of the GF

based PANI electrode, **figure 8 (b)** compares the Nyquist plots of PANI/SS and PANI/3D GF electrodes. A sharp increase of Z_{im} at lower frequency attributed to capacitive behaviour of material however, semi-circle at higher frequencies implies charge transfer resistance (R_{ct}) at electrode/electrolyte interface. Apparently, the PANI/3D GF electrode preserves a much lower resistance than PANI/SS electrode (~10 and ~70 Ω). Thus signifying that the GF based PANI electrode possesses lower contact and charge-transfer impedances. As a result, ion diffusion and electron transfer are accelerated at high cycling rates for the PANI/3D GF electrode. The conventional PANI/SS architecture has self-dimensional restrictions in charge transportation. The 3D graphene network itself can facilitate electron transfer from PANI nanofibers within the whole electrode.

The surface area of PANI nanofibers in contact with the electrolyte solution and their accessibility to charge transfer can influence the capacitance of the system. Actually, in redox process the electrode kinetic limitations causes only the "surface layer" of PANI to contribute in the charge storage mechanism, while the rest part is electrochemically inactive. Hence, in order to overcome this problem, a three-dimensional mesoporous structure is needed.[35-37] Herein, the porous conducting structure of 3D graphene not only offers a large specific surface area for the deposition of PANI nanofibers but also assists electrolyte access subsequently aiding in ion transport to support redox processes. Schematic of charge storage and fast electron transfer in nanofibers PANI-3D graphene backbone is shown in **inset of figure 8 (b)**, results in boosting up capacitance. The PANI deposition easily covers 3D graphene surface. The strong interactions between PANI nanofibers with the 3D graphene surface can support in collection of effective charge for capacitance from the individual PANI nanofibers along the conductive graphene backbone thus increasing the overall

performance of PANI/3D graphene. Compared with PANI/SS, the conductive graphene framework can act as “freeways” for charge transportation between PANI nanofibers, which reduces the inner resistance, hence leading to a better electrode for supercapacitors. The above results show that the PANI on 3D graphene framework can provide a remarkable synergistic augmentation for the improved supercapacitive performance than PANI/SS.

4. Conclusions

In this paper, we reported the facile synthesis of graphene based nanofibers PANI electrode by chemical route. The increased specific capacitance, good cycling stability and improved capability of the PANI/3D GF electrode can be attributed to active PANI nanofibers with large specific surface area and unique graphene structure backbone offering efficient conducting pathways. All above important aspects promote the effectiveness of the 3D graphene framework serving as multifarious booster for superior electrochemical performance. Thus, PANI/3D graphene may be considered as potential candidate for the application in the futuristic energy storage field and this work will expose a new opening for fabrication of 3D graphene-based low cost high performance hybrid materials and/or devices for diverse applications.

Acknowledgement

This research was partially supported by the Futuristic Fundamental Research Program(2E23831-13-095) funded by Korea Institute of Science and Technology, the Pioneer Research Center Program (2010-0019313), and the Priority Research Centers Program (2009-0093823) through the National Research Foundation (NRF) of Korea funded by the Ministry of Science, ICT & Future Planning.

References:

1 P. Simon and Y. Gogotsi, *Nat Mater,* 2008, **7,** 845-854.

2 S. Patra, K. Barai and N. Munichandraiah, *Synth Met,* 2008, **158,** 430-435.

3 S. Cho, K. H. Shin and J. Jang, *ACS Appl Mater Interfaces* 2013, **5**, 9186–9193.

4 A. K. Geim, K. S. Novoselov, *Nat Mater*, 2007, **6,** 183-191.

5 D. A. Dikin, S. Stankovich, E. J. Zimney, R. D. Piner, G. H. Dommett, G. Evmenenko, S. T. Nguyen and R. S. Ruoff, *Nature* , 2007, **448,** 457-460.

6 A. Rochefort and J. D. Wuest, *Langmuir*, 2009, **25,** 210-215.

7 S. Stankovich, D. A. Dikin, G. H. B. Dommett, K. M. Kohlhaas, E. J. Zimney, E. A. Stach, R. D. Piner, S. B. T. Nguyen and R. S. Ruoff, *Nature,* 2006, **442,** 282-286.

8 M. D. Stoller, S. Park, Y. Zhu, J. An and R. S. Ruoff, *Nano Lett,* 2008, **8,** 3498-3502.

9 Z. Chen, W. Ren, L. Gao, B. Liu, S. Pei and H. M. Cheng, *Nat Mater,* 2011, **10,** 424-428.

10 Z. Tai, X. Yan and Q. Xue, *J Electrochem Soc*, 2012, **159,** A1702-A1709.

11 Y. X. Huang, X. C. Dong, Y. Liu, L. J. Li and P. Chen, *J Mater Chem*, 2011, **21,** 12358-12362.

12 S. Y. Yin, Y. Y. Zhang, J. H. Kong, C. J. Zou, C. M. Li, X. H. Lu, J. Ma, F. Y. C. Boey and X. D. Chen, *ACS Nano*, 2011, **5,** 3831-3838.

13 D. Wei and J. Kivioja, *Nanoscale*, 2013, **5**, 10108-10126.

14 S. B. Kulkarni, S. S. Joshi and C.D. Lokhande, *Chem Eng J,* 2011, **166,** 1179-1185.

15 N. V. Blinova, J. Stejskal, M. Trchová and J. Prokeˇs, *Polymer*, 2006, **47**, 42–48.

16 S. Fedorova and J. Stejskal, *Langmuir,* 2002, **18**, 5630–5632.

17 J. Stejskal, M. Trchová, S. Fedorova, I. Sapurina and J. Zemek, *Langmuir* 2003, **19**,

3013–3018.

18 E. Dervishi, Z. Li, F. Watanabe, A. Biswas, Y. Xu, A. R. Biris, V. Sainia and A. S. Biris, *Chem Commun* , 2009, 4061-4063.

19 Ch. Belabed, A. Abdi, Z. Benabdelghani, G. Rekhila, A. Etxeberria, M. Trari, *Int J Hydrogen Energy,* 2013, **38,** 6593-6599.

20 S. B. Kondawar, M. D. Deshpande,S. P. Agrawal, *Int J Comp Mater,* 2012, **2,** 32-36.

21 L. Yan, Y. B. Zheng, F. Zhao, S. Li, X. Gao, B. Xu, P. S. Weiss and Y. Zhao, *Chem Soc Rev*, 2012, **41**, 97–114.

22 A. Grinou, Y. Soo Yun and H. J. Jin, *Macromol Res*, 2012, **20,** 84-92.

23 Y. W. Lee, K. Do, T. H. Lee, S. S. Jeon, W. J. Yoon, C. Kim, J. Ko and S. S. Im, *Synth Met,* 2013, **174,** 6–13.

24 D. Graf, F. Molitor, K. Ensslin, C. Stampfer, A. Jungen, C. Hierold and L. Wirtz, *Nano Lett,* 2007, **7,** 238-242.

25 Y. C. Yong, X. C. Dong, M. B. Chan-Park, H. Song and P. Chen, *ACS Nano,* 2010, **6,** 2394-2400.

26 A. Shakoor, T. Z. Rizvi, A. Nawaz, *J Mater Sci Mater Electron*, 2011, **22,** 1076-1080.

27 J. F. Qiang, Z. H. Yu, H. C. Wu and D. Q. Yun. *Synth Met,* 2008, **158**, 544–547.

28 N. R. Chiou and A. J. Epstein. *Synth Met,* 2005, **153**, 69–72.

29 J. Li, H. Xie, Y. Li, J. Liu, Z. Li, *J Power Sources,* 2011, **196,** 10775–10781.

30 S. B. Kulkarni, A. D. Jagadale, V. S. Kumbhar, R. N. Bulakhe, S. S. Joshi and C. D. Lokhande, *Int J Hydrogen Energy*, 2013, **38,** 4046-4053.

31 U. M. Patil, K. V. Gurav, V. J. Fulari, C. D. Lokhande and O. S. Joo, *J Power Sources,* 2009, **188,** 338-342.

32 L. Li, H. Song, Q. Zhang, J. Yao and X. Chen, *J Power Sources*, 2009, **187,** 268-274.

33 C. Yuan, X. Zhang, L. Hou, L. Shen, D. Li, F. Zhang, C. Fan and J. Li, *J Mater Chem*, 2010, **20**, 10809–10816.

34 V. Khomenko, E. Frackowiak, F. Béguin, *Electrochim Acta,* 2005, **50,** 2499-2506.

35 J. Zang, S. J. Bao, C. M. Li, H. Bian, X. Cui, Q. Bao, C. Q. Sun, J. Guo and K. Lian, *J Phys Chem C*, 2008, **112**, 14843–14847.

36 T. Liu, W. G. Pell and B. E. Conway, *Electrochim Acta*, 1997, **42**, 3541-3552.

37 G. L. Che, B. B. Lakshmi, E. R. Fisher and C. R. Martin, *Nature*, 1998, **393**, 346-349.

Figure captions:

Figure 1: (a) Photograph of chemically deposited PANI on 3D graphene electrode, (b) Schematic reactions and growth mechanism of chemically grown PANI on 3D graphene framework.

Figure 2: XRD pattern of chemically deposited PANI on 3D graphene.

Figure 3: XPS survey spectrum of (a) chemically deposited PANI on 3D graphene. The core level spectra of (b) C1s, (c) N1s. (Black line- original data, Red line– fitted data).

Figure 4: Raman spectrum of chemically deposited PANI on 3D graphene.

Figure 5: FESEM images of (a) 3D graphene framework with (b, c) magnified view, (d) chemically deposited PANI on 3D graphene with (e, f) higher magnification and (g, h, i) overgrown fibers PANI nanostructure.

Figure 6: (a) Comparative cyclic voltammograms of PANI/SS and PANI/3D graphene in aqueous 1M H_2SO_4 at scan rate of 50 mV s^{-1}, (b) Cyclic voltammograms of PANI/3D graphene at different scan rates, (c) The plot of oxidation and reduction peak current versus the square root of scan rate for PANI/3D graphene, (d) Scan rate dependent interfacial and specific capacitance values of PANI/3D graphene electrode.

Figure 7: (a) Comparative galvanostatic charge discharge curves of PANI/SS and PANI/3D graphene at current density of 1 $mAcm^{-2}$, (b) Galvanostatic charge discharge curves of PANI/3D graphene at different charging current densities, (c) charging current density dependent interfacial and specific capacitance of PANI/3D GF electrode, (d) Ragone plot of PANI/3D graphene at different charging current densities. Inset shows Coulombic efficiency at respective current densities.

Figure 8: (a) Stability study of PANI/3D graphene electrode graph of capacity retention ratio for 5,000 cycles, (b) Electrochemical impedance spectrum within 1 MHz to 10 mHz frequency region Nyquist plot of PANI/SS and PANI/3D graphene. Inset shows schematic of charge storage and fast electron transfer in nanofibers PANI-3D graphene.

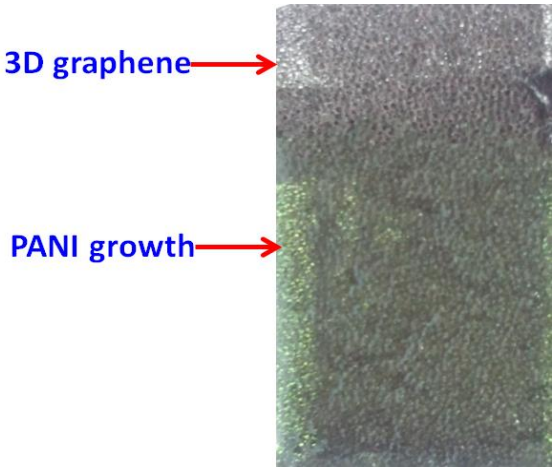

Figure 1 (a)

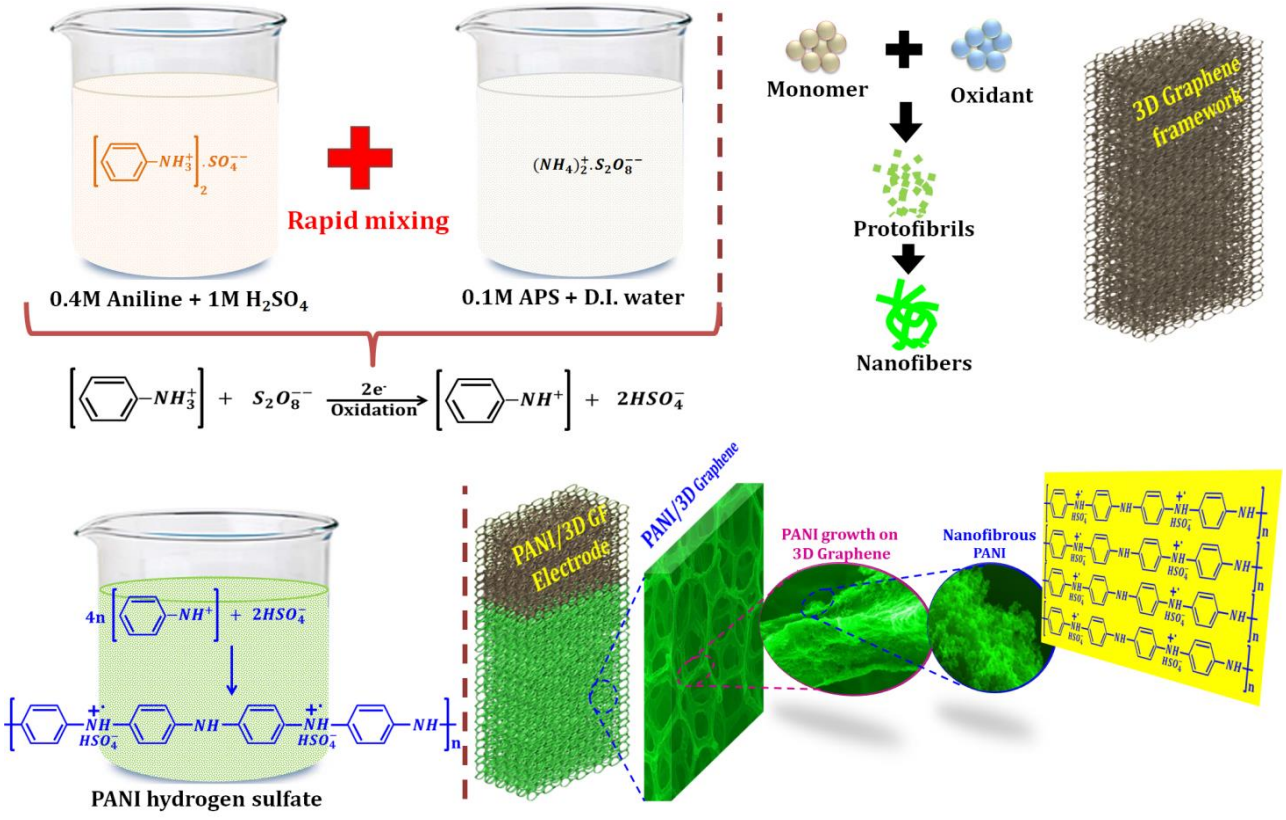

Figure 1 (b)

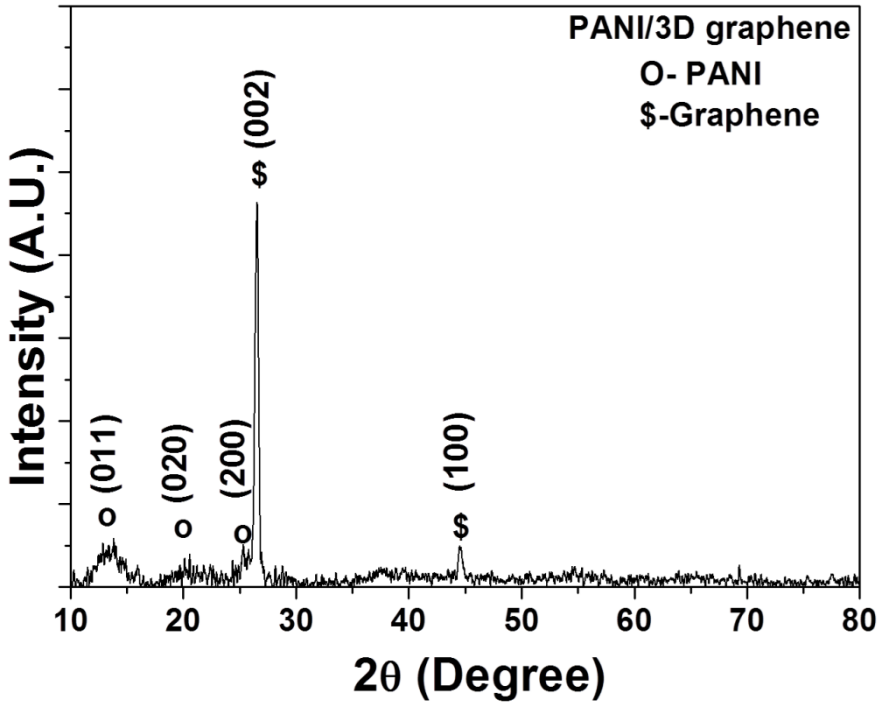

Figure 2

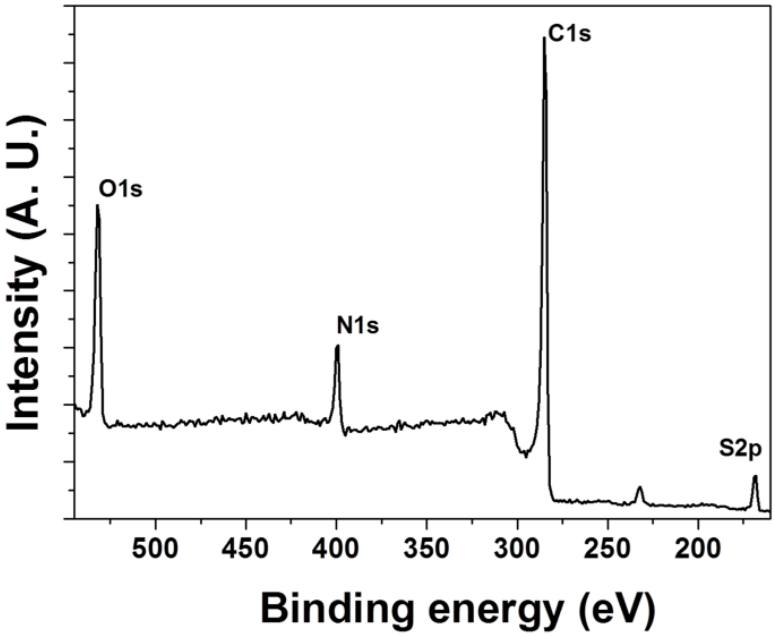

Figure 3 (a)

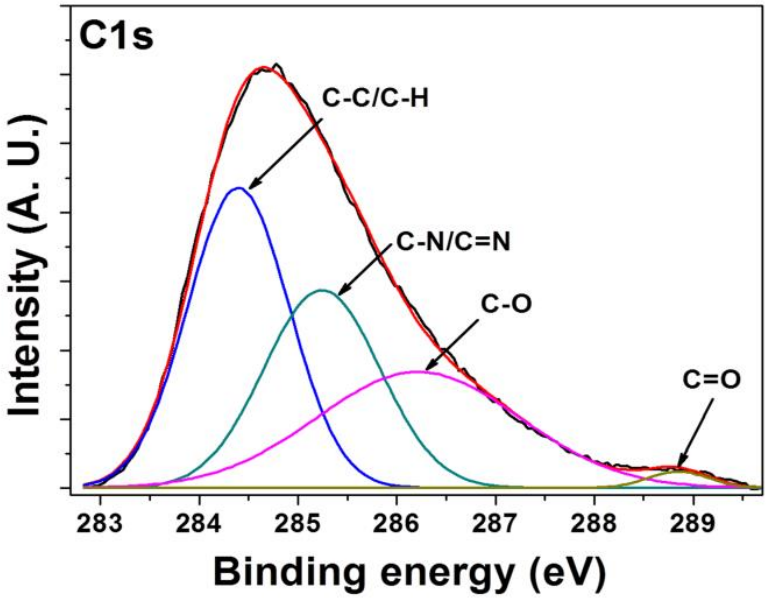

Figure 3 (b)

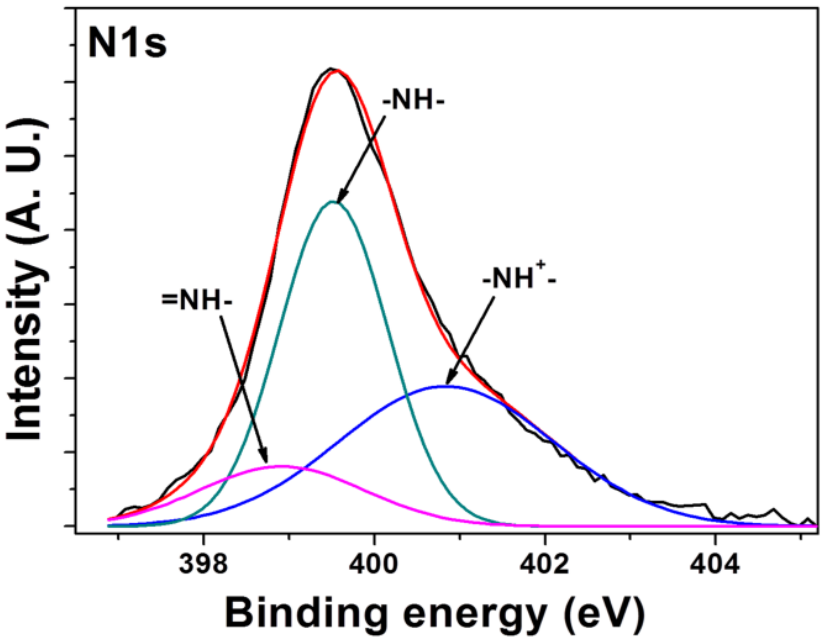

Figure 3 (c)

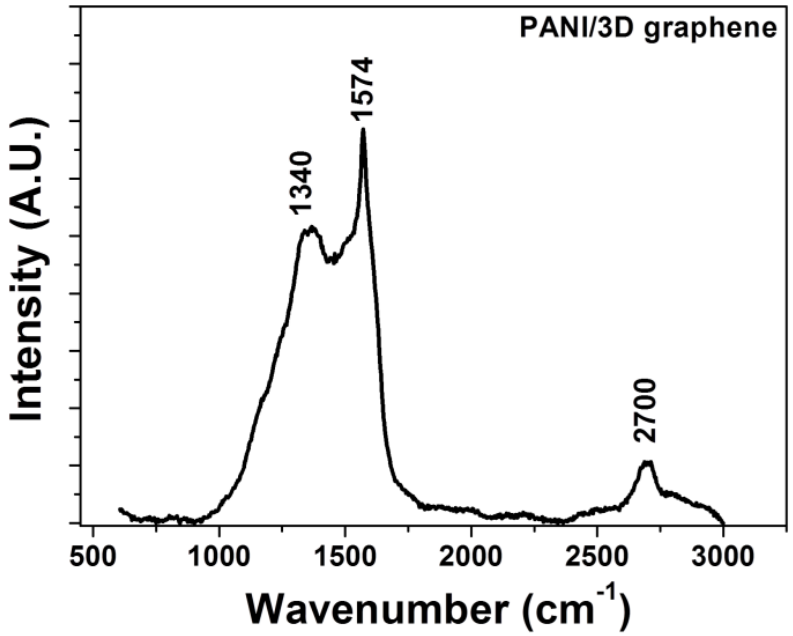

Figure 4

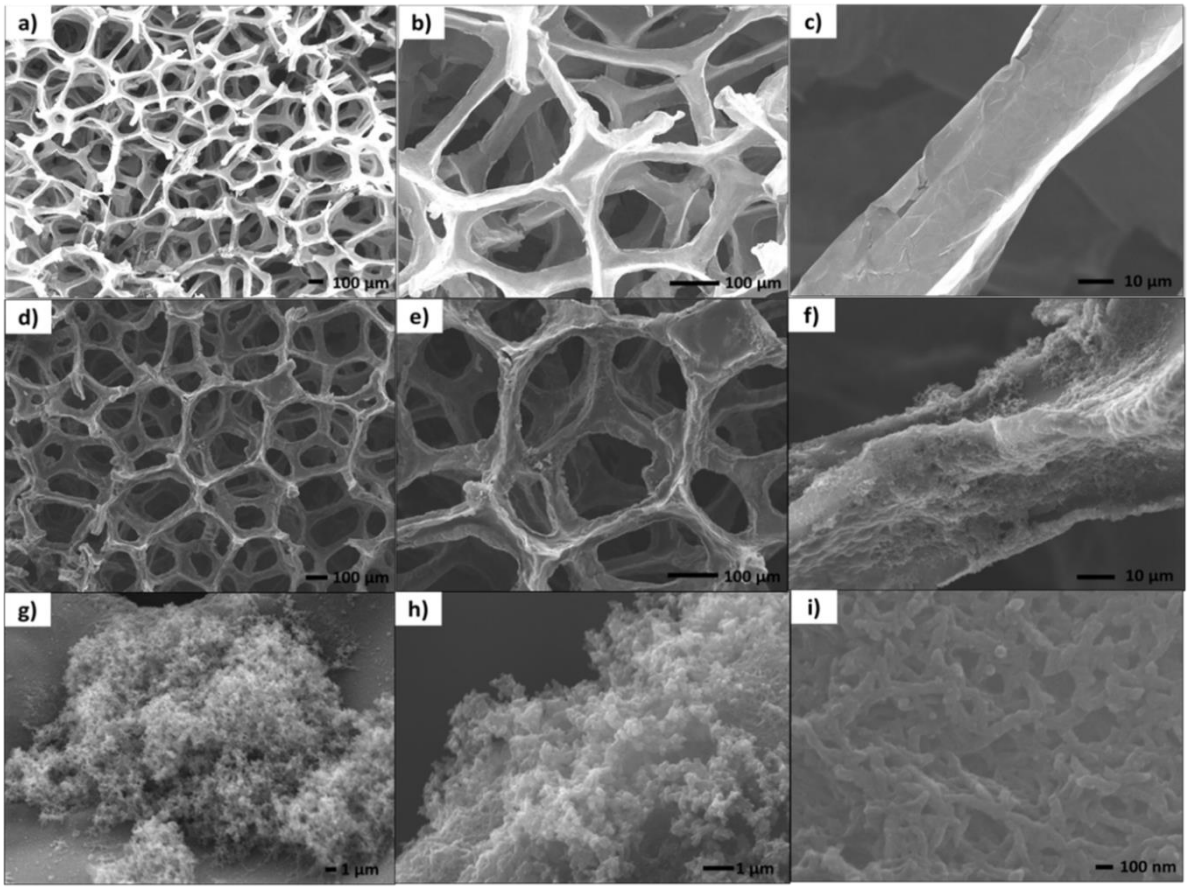

Figure 5

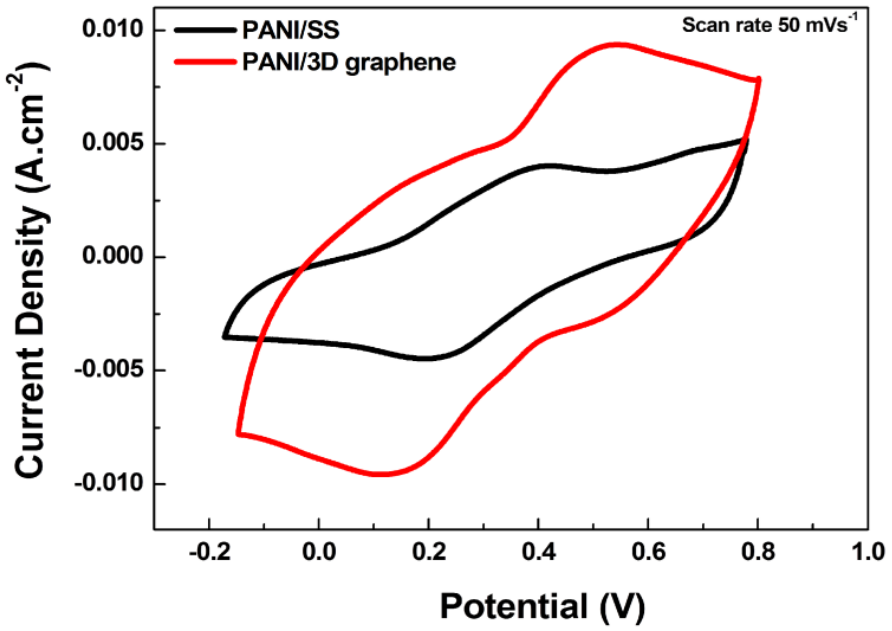

Figure 6 (a)

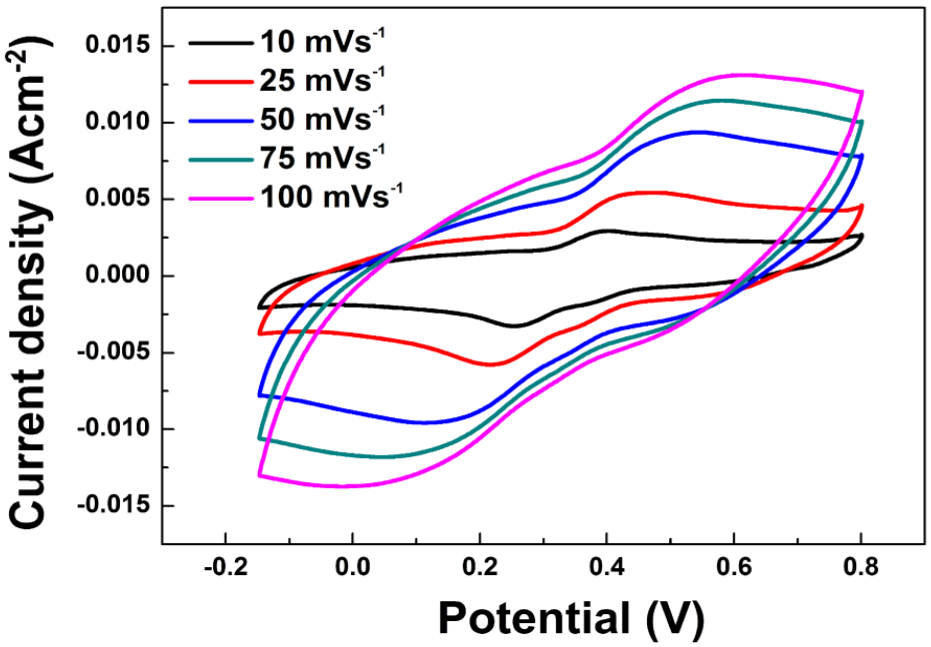

Figure 6 (b)

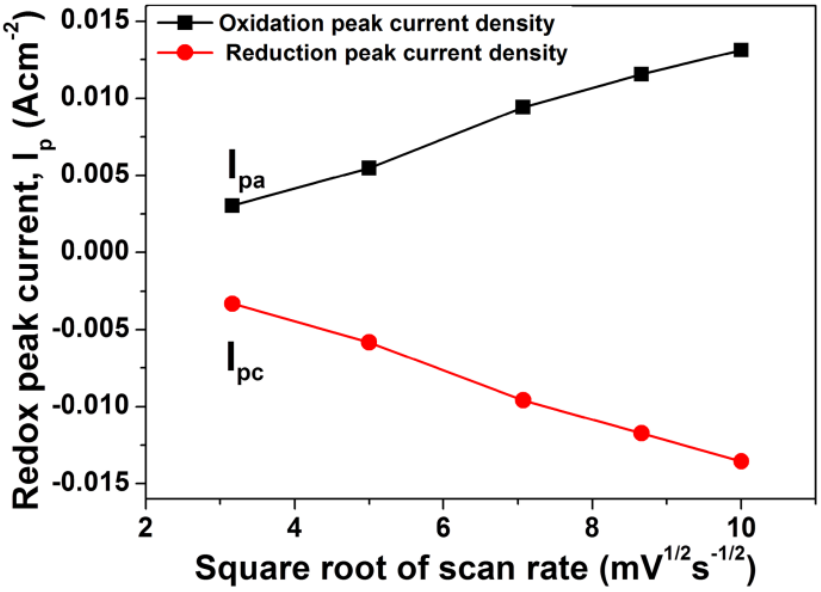

Figure 6 (c)

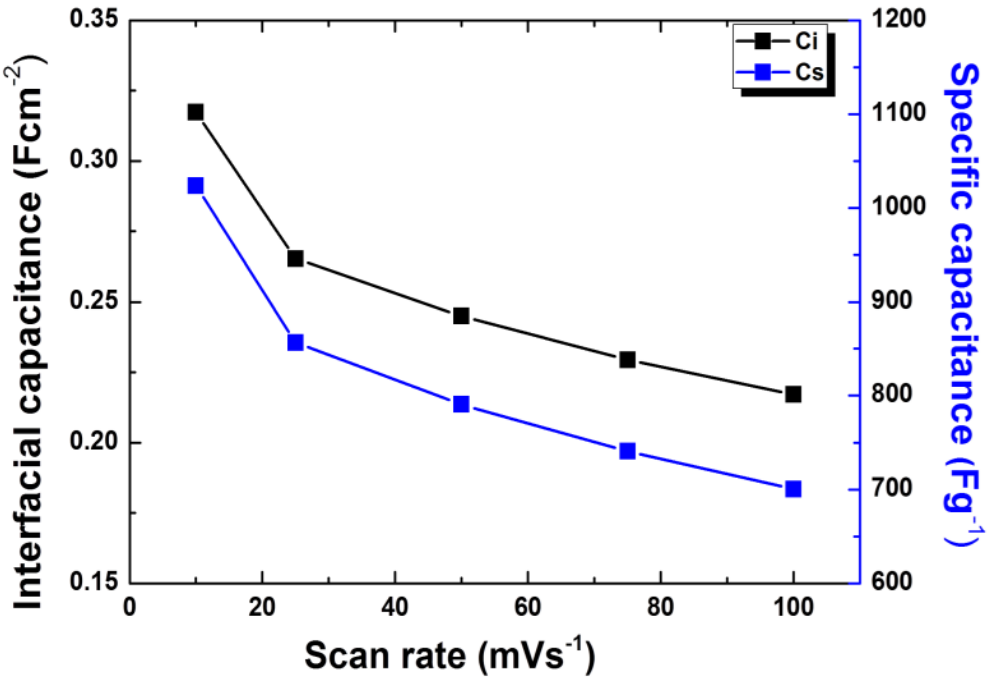

Figure 6 (d)

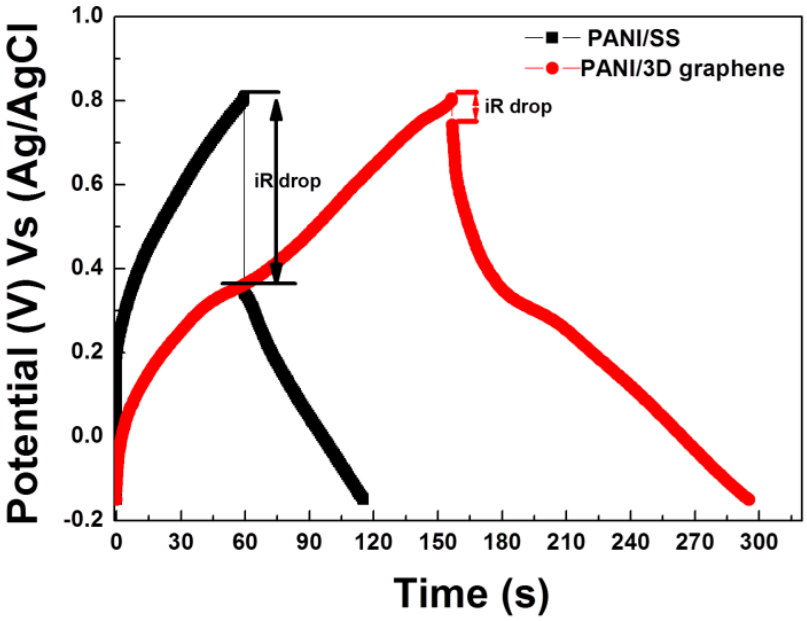

Figure 7 (a)

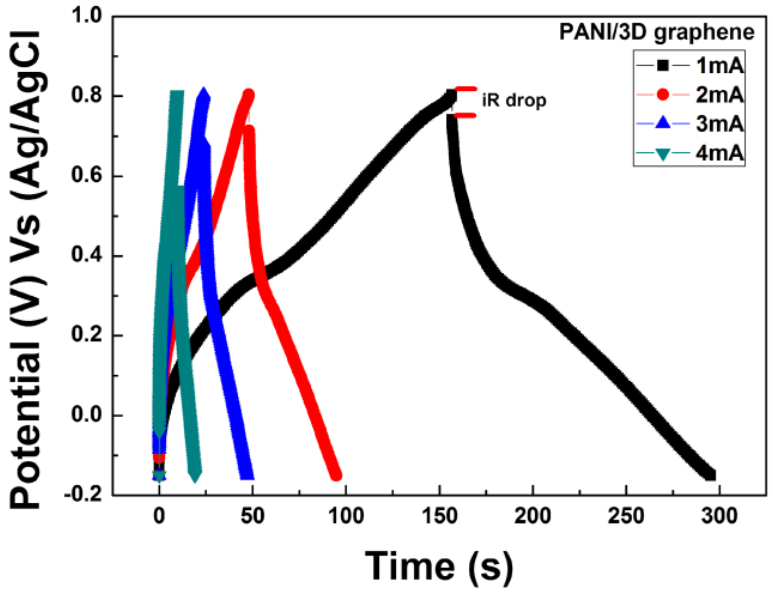

Figure 7 (b)

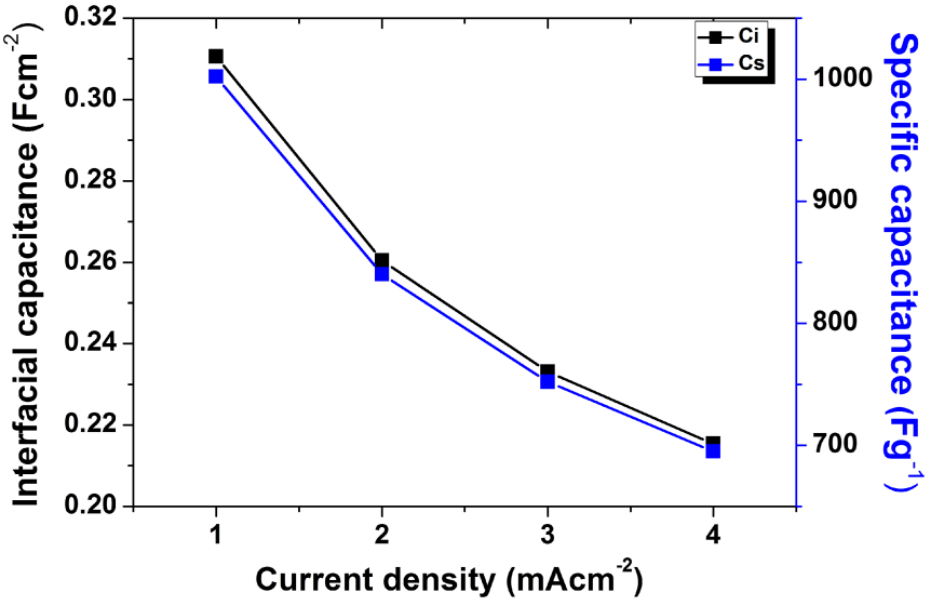

Figure 7 (c)

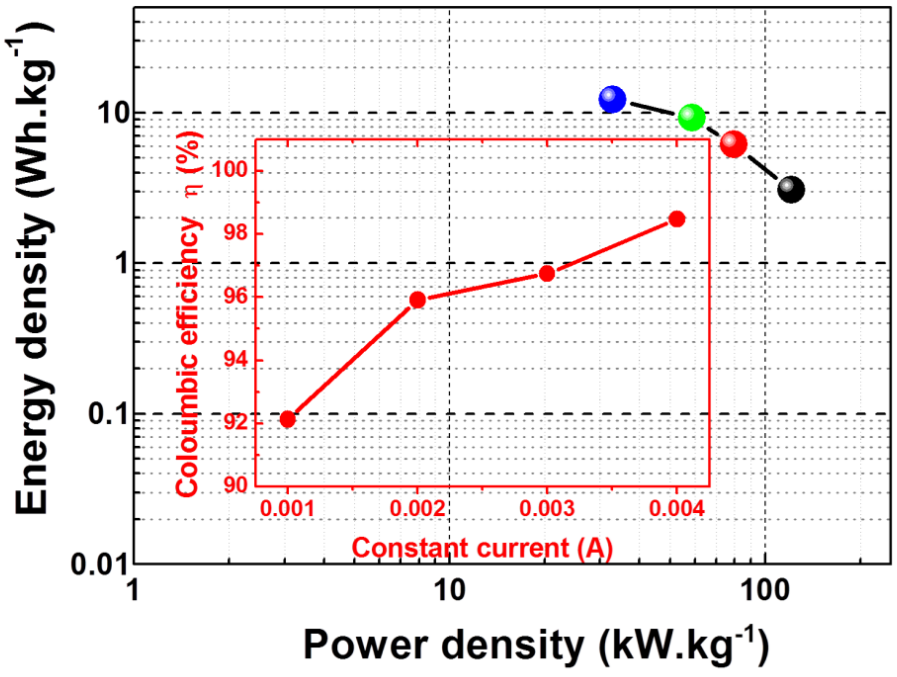

Figure 7 (d)

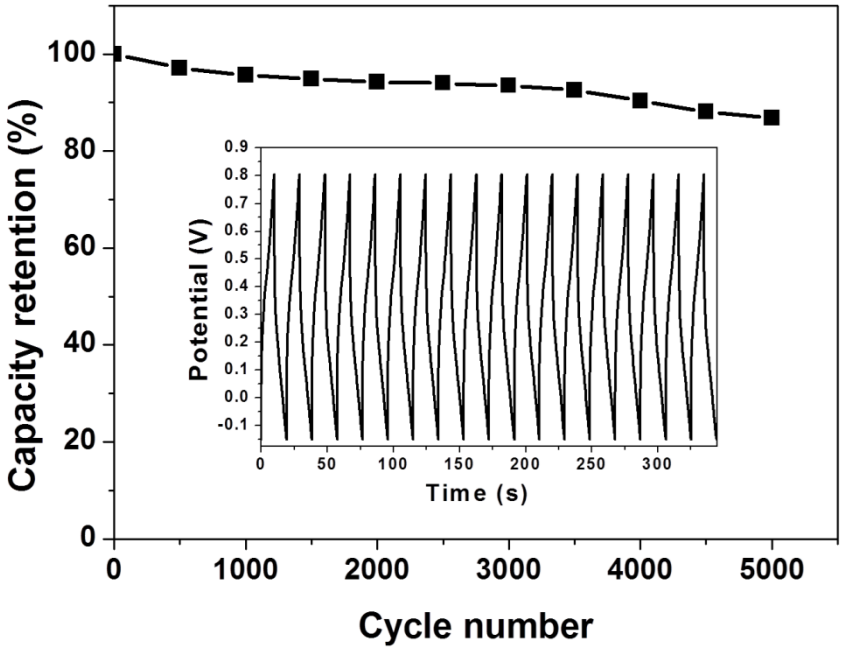

Figure 8 (a)

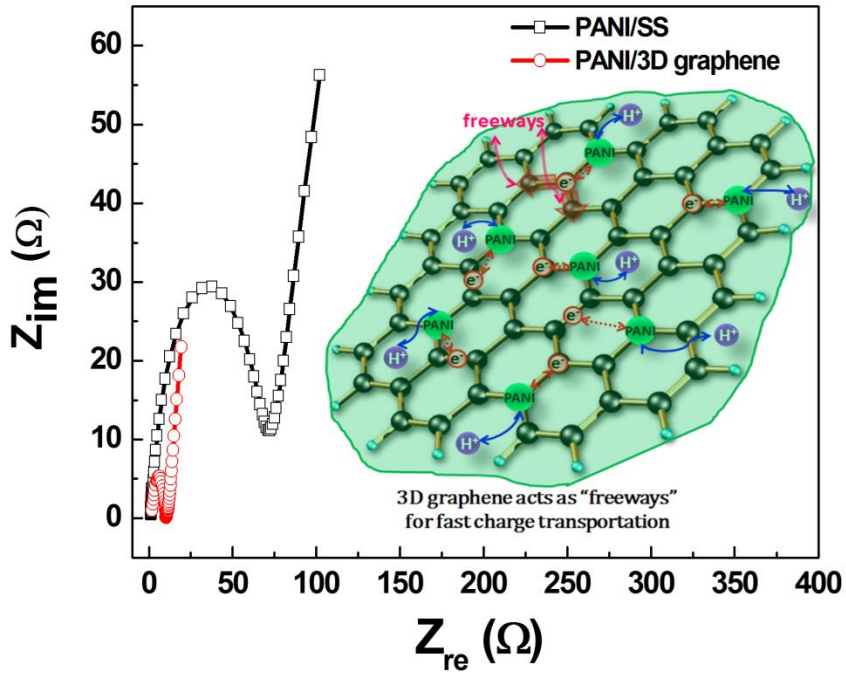

Figure 8 (b)

Supplementary Information

High-performance supercapacitor electrode based on nanofibers polyaniline/3D graphene framework as efficient charge transporter

Sachin B. Kulkarni†, Umakant M. Patil†, Iman Shackery†, Ji Soo Sohn, Suchan Lee, Byeongho Park, SeongChan Jun*

Nano ElectroMechanical Device Laboratory, School of Mechanical Engineering, Yonsei University, Seoul 120-749, Republic of Korea.

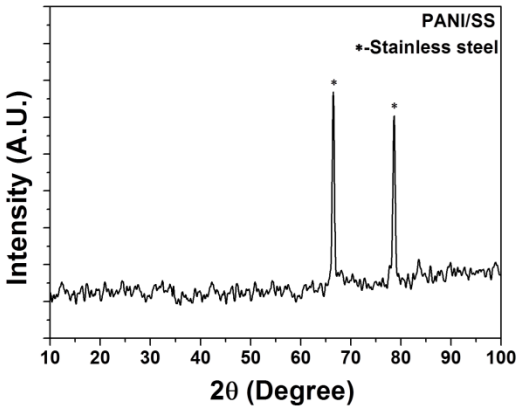

Figure S1: XRD pattern of PANI on stainless steel showing very small peaks indicating less semi-crystalline nature as compared to PANI/3D GF.

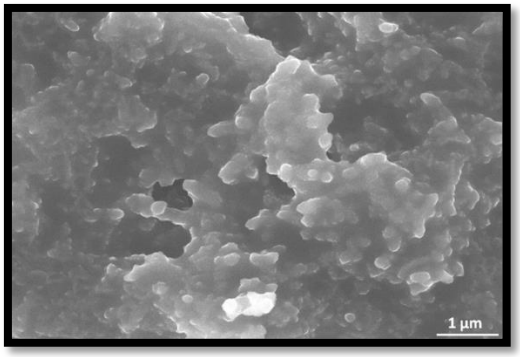

Figure S2: FESEM image of PANI on stainless steel with agglomerated nanofibers, which is in support for lesser semi crystalline PANI growth.

Graphical abstract:

High-performance supercapacitor electrode based on nanofibers polyaniline/3D graphene framework as efficient charge transporter

Sachin B. Kulkarni†, Umakant M. Patil†, Iman Shackery†, Ji Soo Sohn, Suchan Lee, Byeongho Park, SeongChan Jun*

Nano ElectroMechanical Device Laboratory, School of Mechanical Engineering, Yonsei University, Seoul 120-749, Republic of Korea.

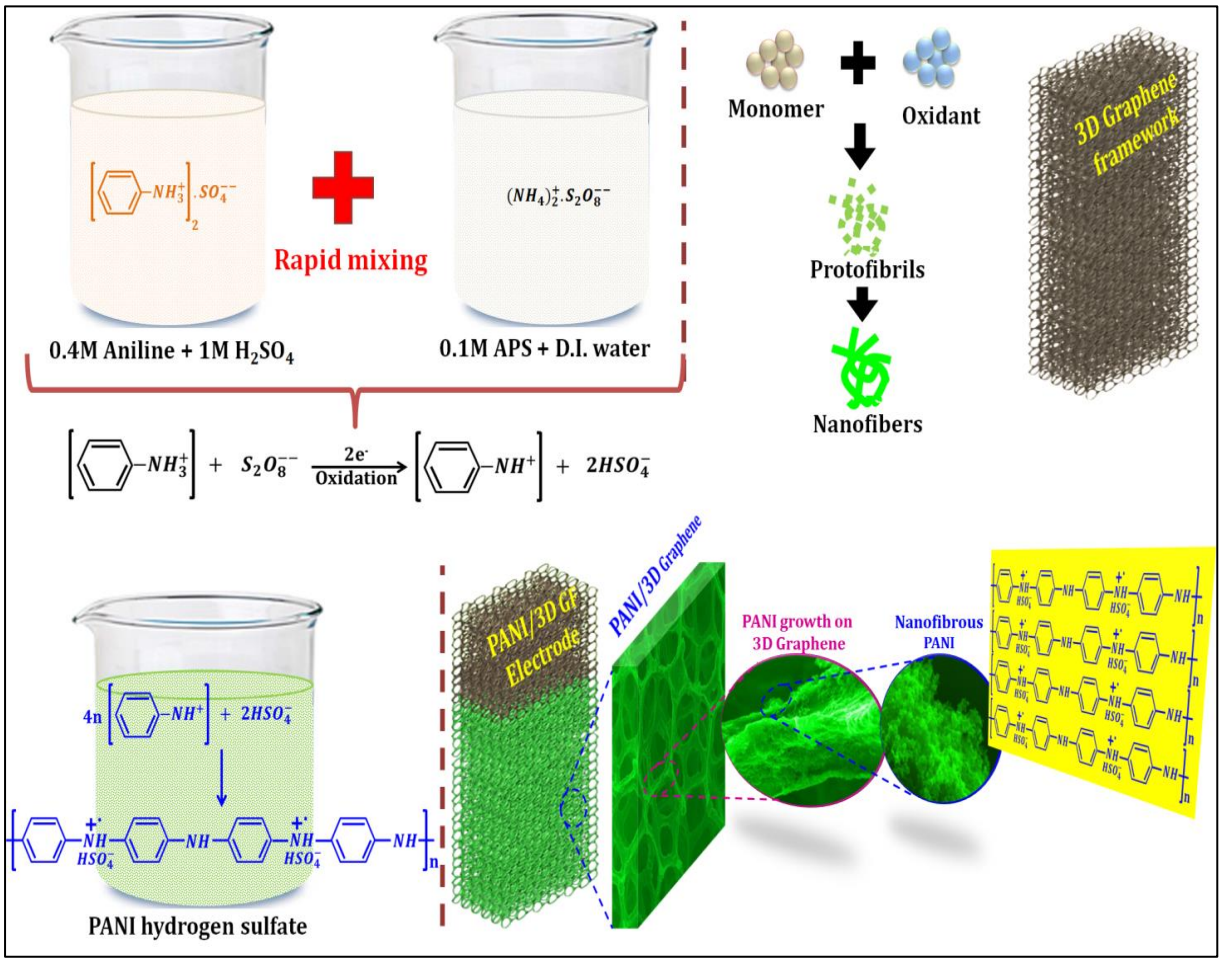

Figure: Schematic and reactions for nanofibers PANI growth via rapid mixing chemical polymerization.

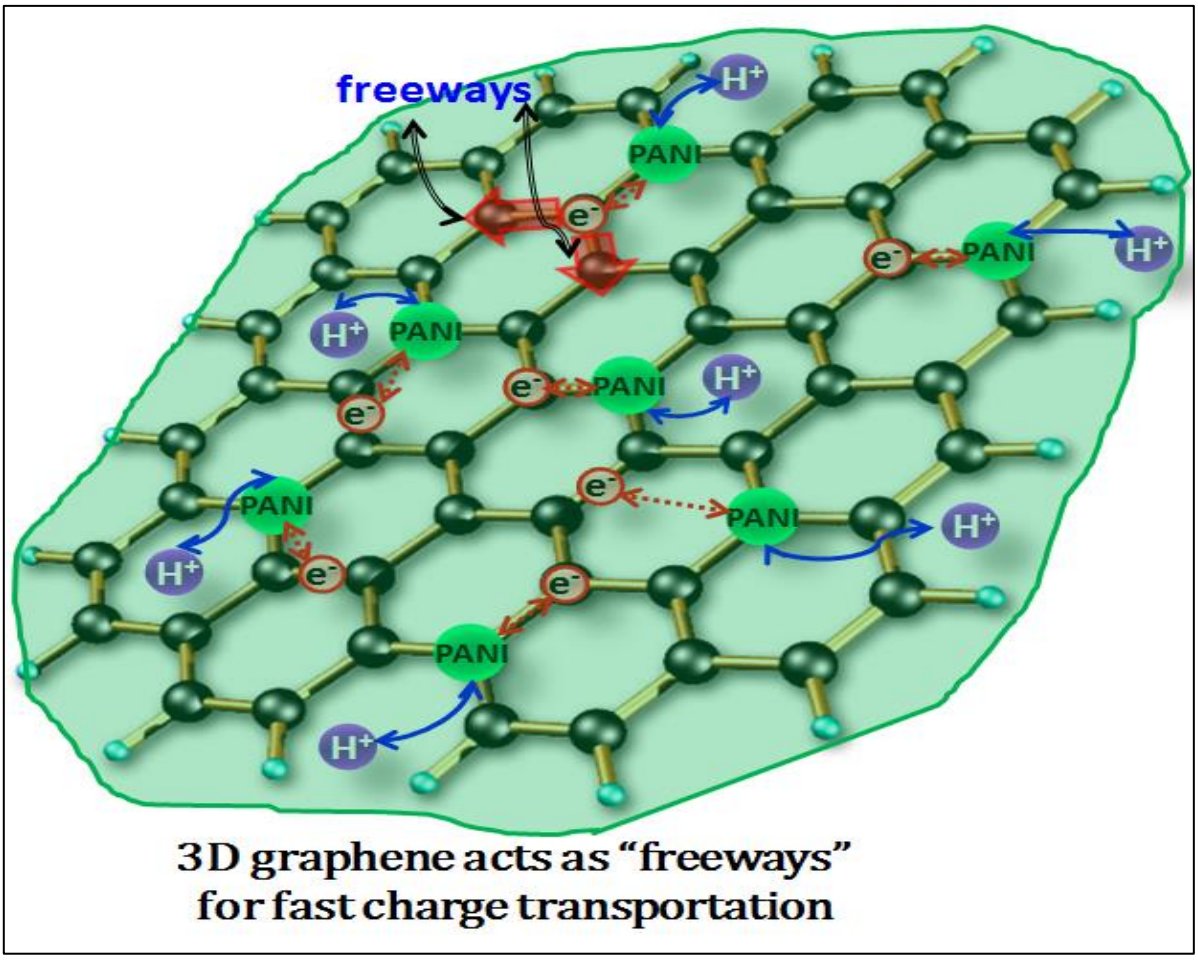

Figure: Schematic of 3D graphene acts as freeways for fast charge transportation.